

# Receptacle Model of Salting-In by Tetramethylammonium Ions

Barbara Hribar-Lee,<sup>\*,†</sup> Ken A. Dill,<sup>‡</sup> and Vojko Vlachy<sup>†</sup>

Faculty of Chemistry and Chemical Technology, University of Ljubljana, Aškerčeva c. 5, SI-1000 Ljubljana, Slovenia, and Department of Pharmaceutical Chemistry, University of California, San Francisco, California 94143-2240, United States

Received: August 25, 2010; Revised Manuscript Received: October 8, 2010

Water is a poor solvent for nonpolar solutes. Water containing ions is an even poorer solvent. According to standard terminology, the tendency of salts to precipitate oils from water is called *salting-out*. However, interestingly, some salt ions, such as tetramethylammonium (TMA), cause instead the *salting-in* of hydrophobic solutes. Even more puzzling, there is a systematic dependence on solute size. TMA causes the salting-out of small hydrophobes and the salting-in of larger nonpolar solutes. We study these effects using NPT Monte Carlo simulations of the Mercedes–Benz (MB) + dipole model of water, which was previously shown to account for hydrophobic effects and ion solubilities in water. The present model gives a structural interpretation for the thermodynamics of salting-in. The TMA structure allows deep penetration by a first shell of waters, the dipoles of which interact electrostatically with the ion. This first water shell sets up a second water shell that is shaped to act as a receptacle that binds the nonpolar solute. In this way, a nonpolar solute can actually bind more tightly to the TMA ion than to another hydrophobe, leading to the increased solubility and salting-in. Such structuring may also explain why molecular ions do not follow the same charge density series as atomic ions do.

## 1. Introduction

Hydrophobic molecules are poorly soluble in water and are typically even less soluble in aqueous solutions that contain salt ions.<sup>1–3</sup> Such multicomponent solutions of water, nonpolar solutes, and salt ions are important throughout many areas of chemistry, including in separations and analytical chemistry; for many types of biomolecules, including proteins, nucleic acids, and lipid bilayers; in formulations of pharmaceuticals; in solutions of micelles and surfactants; and in environmental chemistry.

The first studies of aqueous solutions of salts and nonpolar solutes date back to Franz Hofmeister, who studied how different salts affect the solubilities of proteins in water.<sup>4,5</sup> Salting-in and salting-out are now commonly used techniques in protein separation technology. The reduction in solubilities of hydrophobic solutes in water due to the presence of salts is described by the empirical Setschenov equation<sup>6</sup>

$$\ln \frac{c_i}{c_i(0)} = -k_S c_S \quad (1)$$

where  $c_i$  and  $c_i(0)$  are the molar solubilities of the hydrophobe in a salt solution and in water, respectively;  $c_S$  is the molar concentration of the salt; and  $k_S$  is the salt's Setschenov salting-out coefficient. The value of  $k_S$  depends on the type of salt and the nature of the nonelectrolyte.<sup>2,7–9</sup> The “Hofmeister series” is a rank-ordering of ion types based on the values of their Setschenov coefficients.<sup>10–12</sup>

Interestingly, while most monatomic inorganic ions have a positive value of  $k_S$ —salts usually drive hydrophobes to pre-

cipitate in water—a few molecular ions have  $k_S < 0$ .<sup>13</sup> For example, tetraalkylammonium salts<sup>2,8,9,14–16</sup> tend to favor dissolving hydrophobes in water. This is called *salting-in*. A similar effect has been observed for certain alcohols.<sup>9,17–19</sup>

Several mechanisms have been proposed to explain the effect of electrolytes on the properties of hydrophobes in aqueous solutions.<sup>3,20–22</sup> The first explanation proposed by Hofmeister<sup>4</sup> suggests that ions get strongly hydrated removing the water molecules from the hydration shell of the hydrophobes, leading to salting-out. Other models related the salting-out effect with the contraction of the volume upon dissolving most of the electrolytes in water. These theories are based on the fact that the Setschenov coefficient of a salt correlates with how that salt changes the volume of the solution,  $V_S - \bar{V}_S^0$ , where  $\bar{V}_S^0$  is the partial molar volume of the salt at infinite dilution and  $V_S$  is the molar volume of the salt as in the molten state.<sup>3</sup> Salting-in occurs if  $V_S - \bar{V}_S^0$  is negative.<sup>3,7,16</sup> It is also known that salt effects on nonpolar solubilities depend on the charge densities of the salt ions. Ions having high charge densities (they are small in size or have high charge) tend to reduce the hydrophobic solubilities in water (salting-out effect, positive  $k_S$ ), whereas ions having low charge densities (large ions or small charge) tend to increase the solubilities of hydrophobes (salting-in effect, negative  $k_S$ ). While these approaches can predict the relative efficiency of ions as salting-out agents, they fail to explain the salt-induced increase of the hydrophobe solubility, as well as different effects of a particular salt on different hydrophobic molecules.

Computer simulations have been performed to seek a more microscopic and structural interpretation of ion–hydrophobe interactions in water<sup>7,20,23–27</sup> to resolve these questions. It has been shown that the salting-in and salting-out effects can be correlated to the hydrophobe hydration in electrolyte solutions versus the hydration in pure water. Ions of high charge density, classified as kosmotropes, are strongly hydrated and cannot

\* Corresponding author. E-mail: barbara.hribar@fkkt.uni-lj.si.

<sup>†</sup> University of Ljubljana.

<sup>‡</sup> University of California.

come into direct contact with the hydrophobe, leading to the salting-out effect. The opposite is true for the chaotropic ions that exhibit hydrophobe-like character.<sup>24,28</sup> They are weakly hydrated and can come into direct contact with hydrophobe, leading to salting-in. This association requires an opening of a solute-size cavity in the first hydration shell of the ion. This process is being opposed by the entropic cost in the case of kosmotropes but is entropy driven in the case of chaotropes.<sup>28</sup> In addition, the salting-in process is reinforced by a favorable solute–solvent energy change. Along these lines, the importance of the hydrophobe geometrical properties can be understood.

The specific value of  $k_S$  for a certain salt depends on the size and shape of the hydrophobe<sup>2,8,9,29</sup> and is correlated with the molecular volume of the latter.<sup>3,30</sup> In some cases, the same salt will salt-out small hydrophobes (positive  $k_S$ ) but will salt-in large hydrophobes.<sup>8</sup>

Recent molecular dynamics and Monte Carlo simulations indicate that the salting-out effect caused by small ions is due to the exclusion of the hydrophobe from the ion's first water shell.<sup>23,24,27,31</sup> The hydrophobe, depending on its size, inserts either into the first water shell around the ion or into the second water shell. Small ions bind water tightly, so the hydrophobe is excluded from their first solvation shell, driving salting-out of the hydrophobes.<sup>27</sup> The effect is more pronounced for large hydrophobes. This finding is consistent with the experimental studies of solubility of hydrophobic solutes.<sup>32</sup> Zhang and Cremer<sup>32</sup> found that the Hofmeister effect is caused by the change in the hydration water structure due to the presence of the salt. These findings were confirmed also by recent computer simulations.<sup>33,34</sup>

What remains largely unexplored, however, is the mechanism of salting-in. This is the purpose of the present study. We use here the Mercedes-Benz (MB) model of water.<sup>35,36</sup> Despite its simplicity, this two-dimensional (2D) model correctly reproduces many properties of water and aqueous solutions. Interestingly, the two-dimensional and three-dimensional version<sup>37</sup> of the model provide the same insights into the water properties. Because the 2D MB model has previously been shown to correctly explain the qualitative behavior of the Setschenov salting-out coefficients for simple hydrophobes of different sizes in the presence of different simple salts,<sup>27,31</sup> it provides a good basis for our present exploration of salting-in. Review of experimental data for  $k_S$  values<sup>7</sup> shows that tetramethylammonium bromide in water salts-in most of the hydrophobes and has a negative value of  $V_S - \bar{V}_S^0$  (−16 mL/mol), so it is a useful paradigmatic salt for the present study.

## 2. Model Description and the Simulation

In the two-dimensional MB + dipole model, each water molecule is represented as a disk that interacts with other molecules through a Lennard-Jones (LJ) interaction and through an orientational-dependent hydrogen-bonding (HB) interaction.<sup>25,27,35,36</sup> The name arises because there are three hydrogen-bonding arms, arranged as in the Mercedes-Benz logo (cf. Figure 1a).

In the MB model, the energy of interaction between two waters is<sup>35</sup>

$$U^{\text{ww}}(\mathbf{X}_i, \mathbf{X}_j) = U_{\text{LJ}}(r_{ij}) + U_{\text{HB}}(\mathbf{X}_i, \mathbf{X}_j) \quad (2)$$

The notation is the same as in previous papers:<sup>25,27,35,36</sup>  $\mathbf{X}_i$  denotes a vector representing both the coordinates and the orientation of the  $i$ th water molecule, and  $r_{ij}$  is the distance

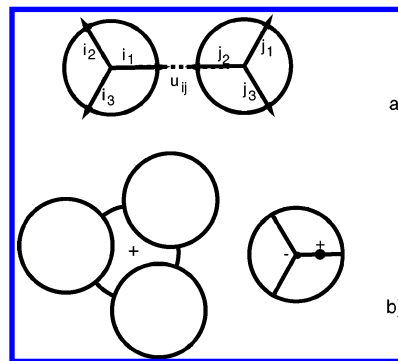


**Figure 1.** MB–dipole model: the water–water and water–tetramethylammonium ion interaction.

between the molecular centers of the molecules  $i$  and  $j$ . The Lennard-Jones term is

$$U_{\text{LJ}}(r_{ij}) = 4\epsilon_{\text{LJ}} \left[ \left( \frac{\sigma_{\text{LJ}}}{r_{ij}} \right)^{12} - \left( \frac{\sigma_{\text{LJ}}}{r_{ij}} \right)^6 \right] \quad (3)$$

where  $\epsilon_{\text{LJ}}$  and  $\sigma_{\text{LJ}}$  are the well-depth and contact parameters, respectively. In addition, neighboring water molecules can form an explicit hydrogen bond when an arm of one molecule aligns with an arm of another water molecule, with an energy function that is a Gaussian function of separation and angle

$$U_{\text{HB}}(\mathbf{X}_i, \mathbf{X}_j) = \epsilon_{\text{HB}} G(r_{ij} - r_{\text{HB}}) \sum_{k,l=1}^3 G(\mathbf{i}_k \cdot \mathbf{u}_{ij} - 1) \times G(\mathbf{j}_l \cdot \mathbf{u}_{ij} + 1) \quad (4)$$

where  $G(x)$  is an unnormalized Gaussian function

$$G(x) = \exp[-x^2/2\sigma^2] \quad (5)$$

The unit vector  $\mathbf{i}_k$  represents the  $k$ th arm on the  $i$ th particle ( $k = 1, 2, 3$ ), and  $\mathbf{u}_{ij}$  is the vector joining the center of molecule  $i$  to the center of molecule  $j$  (Figure 1a). H-bonding arms are not distinguished as donors and acceptors. The strength of the hydrogen bond is only determined by the degree of the arm's alignment.<sup>35</sup>

The model parameters are defined as previously.<sup>25,27,35,36</sup> The parameters  $\epsilon_{\text{HB}} = 1$  and  $r_{\text{HB}} = 1$  define the optimal hydrogen bond energy and bond length, respectively. The same width parameter  $\sigma = 0.085$  is used for both the distance and the angle deviation of a hydrogen bond. The interaction energy in the Lennard-Jones potential function,  $\epsilon_{\text{LJ}} = 0.1\epsilon_{\text{HB}}$ , and the LJ distance,  $\sigma_{\text{LJ}}$ , is 0.7 of that of  $r_{\text{HB}}$ . The MB model was modified to include an electrostatic dipole.<sup>27</sup> A single negative charge is put at the center of each water molecule, and a single positive charge is put onto one of the H-bonding arms, at a distance  $0.165 r_{\text{HB}}$  from the center (Figure 1b). An ion interacts with the charges on a water molecule through a screened potential

$$U_{\text{charge}} = z_i z_j \epsilon_{\text{HB}} |\alpha| \frac{\exp(-\kappa r_{ij})}{r_{ij}} \quad (6)$$

Here,  $r_{ij}$  is the distance between the ion center and a charge on a water dipole, and the valencies  $z_i(z_j)$  are +1 and −1. All the distances are in the units of  $r_{\text{HB}}$ . The parameter  $\kappa$  is, as

**TABLE 1: Free Energy of Insertion,  $\Delta G_{\text{ins}}$ , of Hydrophobes of Different Sizes into Pure Water and into the Water with a Single TMA Ion, as Obtained from Our Monte Carlo Simulation**

$\sigma_{\text{LJ,hyd}}$	$\Delta G_{\text{ins}}/k_{\text{B}}T$ (pure water)	$\Delta G_{\text{ins}}/k_{\text{B}}T$ (water + TMA)	$\Delta\Delta G/k_{\text{B}}T$
0.7	$1.26 \pm 0.01$	$1.30 \pm 0.01$	+0.04
1.2	$2.76 \pm 0.01$	$2.76 \pm 0.01$	0.00
1.5	$3.86 \pm 0.02$	$3.82 \pm 0.02$	-0.04
1.8	$4.90 \pm 0.02$	$4.84 \pm 0.03$	-0.06
2.0	$5.58 \pm 0.04$	$5.50 \pm 0.04$	-0.08

previously established,<sup>27</sup> 0.1, and  $\alpha = 2.27$ . The ion–water potential is

$$U^{i\text{w}}(\mathbf{X}_i, \mathbf{X}_j) = U_{\text{LJ}}(r_{ij}) + \sum_{+,-} U_{\text{charge}}(\mathbf{X}_i, \mathbf{X}_j) \quad (7)$$

We modeled different hydrophobic solutes as disks of different diameters ( $\sigma_{\text{hyd}}$ ).<sup>31</sup> The tetramethylammonium ion is modeled as shown in Figure 1b. The nitrogen atom is a central disk having the same diameter as water ( $\sigma_{\text{LJ}} = 0.7$ ), with a positive charge at its center. The three methyl groups are disks of the same size intercepting the central sphere at a distance 0.5 from the center (Figure 1b). Only the central disk has a charge, but all the disks interact with waters and with the hydrophobe molecule through a Lennard-Jones potential. The well-depth for the Lennard-Jones potential,  $\varepsilon_{\text{LJ}}$ , is, as before,<sup>27</sup> taken to be the same for all the molecules,  $\varepsilon_{\text{LJ}} = 0.1\varepsilon_{\text{HB}}$ .

The Monte Carlo simulations were performed at constant pressure ( $P^* = Pr_{\text{HB}}^2/\varepsilon_{\text{HB}} = 0.19$ ) in the *NPT* ensemble. Monte Carlo steps were displacements and rotations of the water molecules. The simulations were performed using 60 water molecules and a single TMA ion fixed in the center of the simulation box. The first  $10^8$  steps were used to equilibrate the system, and the statistics were collected over the following  $5 \times 10^8$  steps. After the system was equilibrated, the free energy, enthalpy, and entropy of transferring a hydrophobe into a solution were calculated using the Widom test-particle method<sup>38</sup> and using related fluctuation formulas.<sup>35</sup> The potential of mean force between the ion and a nonpolar solute was calculated using the Widom method.<sup>27,38</sup>

### 3. Results and Discussion

To validate our model, we first show that it correctly predicts salting-in for the TMA ion, while predicting salting-out for other simpler ions. The free energy of transfer of simple hydrophobic solutes of different sizes was calculated using the Widom method.<sup>27,38</sup> We compare experiments, which are given in terms of  $k_{\text{S}}$ , with the underlying corresponding quantity<sup>27,31</sup> from our model,  $\Delta\Delta G$ , the difference in free energy between transfer into solution vs pure water. The comparison is shown in Table 1 and Figure 2. The upper panel of Figure 2 shows experimental  $k_{\text{S}}$  for hydrocarbon gases (dashed line<sup>9</sup>) and 2-ketones (solid lines<sup>8,39</sup>) in aqueous solutions of different salts. The lower panel shows the results for the  $\Delta\Delta G$  of hydrophobes of different sizes in the presence of a sodium ion<sup>31</sup> and a TMA ion (this work). Note that while the experimental values for  $k_{\text{S}}$  are given for salts the calculated values are given for single ions. It has been established previously that the cation and anion effects on the hydrophobe solubility are independent and additive.<sup>18,40</sup>

While there is a slight tendency for small hydrophobes ( $\sigma_{\text{LJ}} = 0.7$ ) to be salted out (small positive value for  $\Delta\Delta G$ )

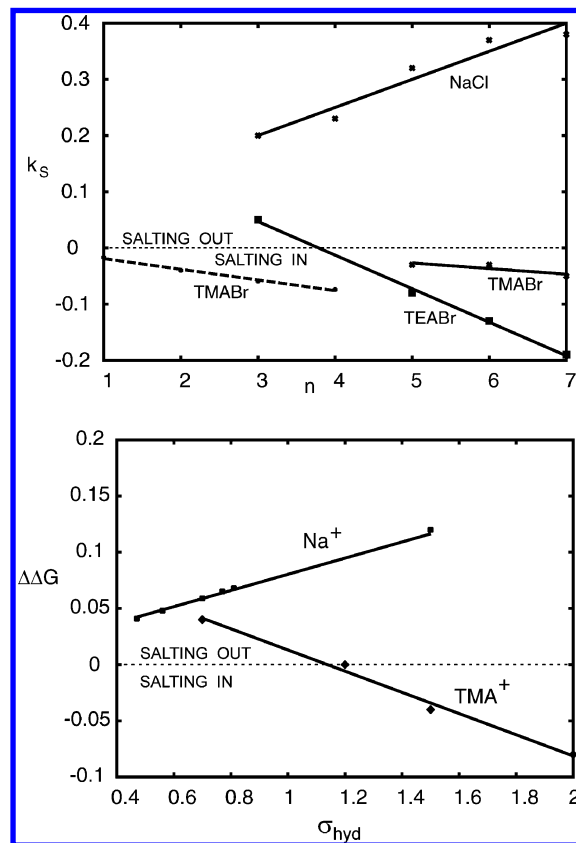


**Figure 2.** Experimental Setchenov coefficients,  $k_{\text{S}}$ , in mol/kg for different salts as a function of a hydrophobe size (upper panel) and  $\Delta\Delta G/k_{\text{B}}T$  as obtained with the MB + dipole TMA model (lower panel). The experimental data for hydrocarbon gases (from ref 9) are shown by a dashed line, and the data for 2-ketones (from refs 8, 39) are shown by solid lines.  $n$  denotes the number of carbon atoms in a molecule.

regardless of the salt, the TMA model ion increases the solubility of larger hydrophobes, roughly beyond the size of benzene (e.g.,  $\sigma_{\text{LJ}} = 1.5$  in our model). This is in qualitative agreement with the experimental value of  $k_{\text{S}} = -0.24$  for the salting-in of the benzene in aqueous solution of TMA–bromide.<sup>2</sup> The  $\Delta\Delta G$  value slightly decreases with the hydrophobe size as shown experimentally for  $k_{\text{S}}$ , for example, for hydrocarbon gases<sup>9</sup> or 2-ketones<sup>8</sup> in aqueous TMA salt solutions (Figure 2). The model correctly captures the trends of  $k_{\text{S}}$  with the size of the nonpolar solute for both salting-in and salting-out salts.

It is worth mentioning here that even certain salts consisting of two large simple ions, such as CsI, salt-in hydrophobes of considerable size, such as benzene.  $k_{\text{S}}$  for benzene in water solutions of CsI is reported to be a small negative value,  $-0.006^3$  (note that we also get a small negative value for  $\Delta\Delta G$  ( $-0.02$ ) of benzene-size hydrophobes in the presence of a model Cs ion). However, due to a limited amount of experimental data on cesium salts, we decided to use TMA as a reference ion in our study.

A more stringent test of our model is the temperature dependence of  $k_{\text{S}}$ . Figure 3 shows our predictions vs experiments for gaseous methane and ethane in TMABr water,<sup>9</sup> which we model using two different hydrophobe sizes,  $\sigma_{\text{hyd}} = 1.2$  and  $\sigma_{\text{hyd}} = 1.5$ . Our model correctly captures the three main properties: (1) that  $k_{\text{S}}$  decreases with temperature, (2) that this can cause a crossover from salting-out to salting-in, and (3) that  $k_{\text{S}}$  is more negative for the larger solute.

Now, we explore the microscopic basis for these results. Figure 4 shows the structure of water around the tetramethy-

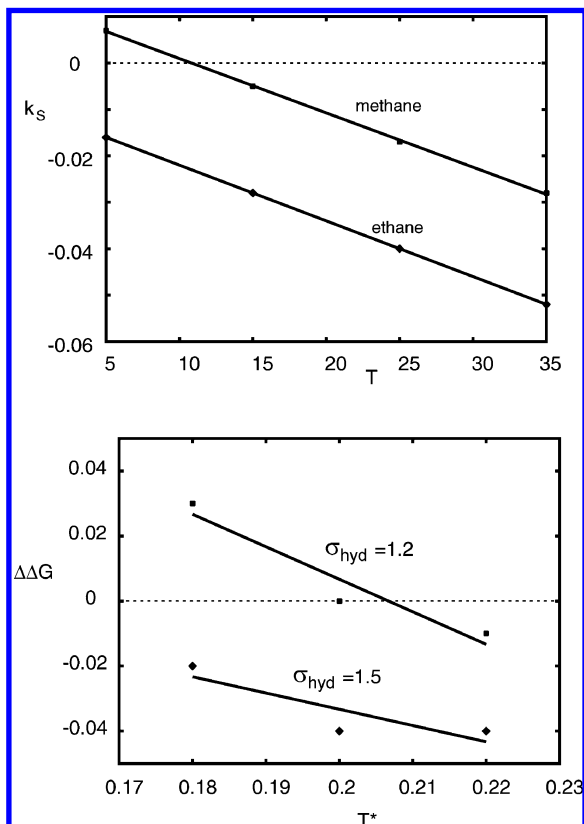


**Figure 3.** Experimental Setchenov coefficients,  $k_s$ , in mol/kg, for gaseous methane and ethane in water TMABr solution as a function of temperature (from ref 9) (upper panel) and  $\Delta\Delta G/k_B T$  as obtained with the MB + dipole TMA model for two different hydrophobe sizes (lower panel).

lammonium ion in our model. Figure 4, left panel, shows the angle-averaged TMA–water pair distribution function, and Figure 4, right panel, shows the relative water density around the TMA ion. The first notable feature is very high density of water molecules that wedge in between the methyl groups of the TMA ion (yellow areas in the lower panel of Figure 4). There is also a high probability of finding a water molecule in the vicinity of the methyl groups (at an approximate distance 1.2 from the center of the TMA ion). This is in qualitative agreement with the results obtained by molecular dynamics study of more realistic all-atom models,<sup>41–43</sup> as well as with the experimental data.<sup>44,45</sup> In these previous studies, it was also found that water molecules prefer to occupy the space between the methyl groups as well as that waters form traditional

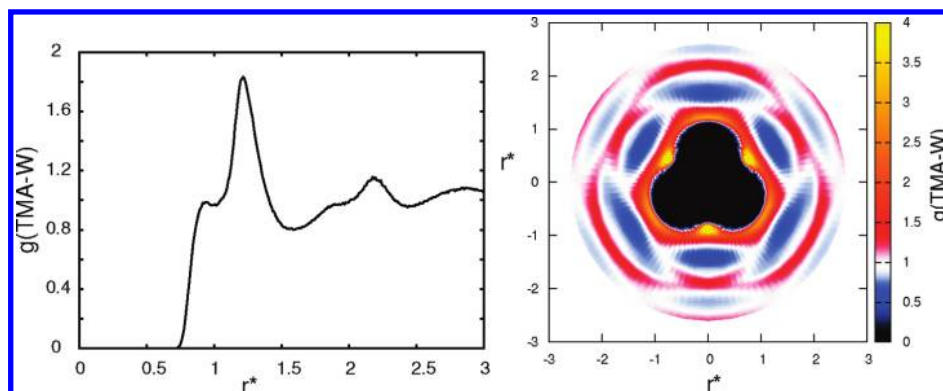


**Figure 4.** Average (left panel) and orientation-dependent (right panel) water–tetramethylammonium ion pair distribution function as obtained from MC simulation for MB + dipole.

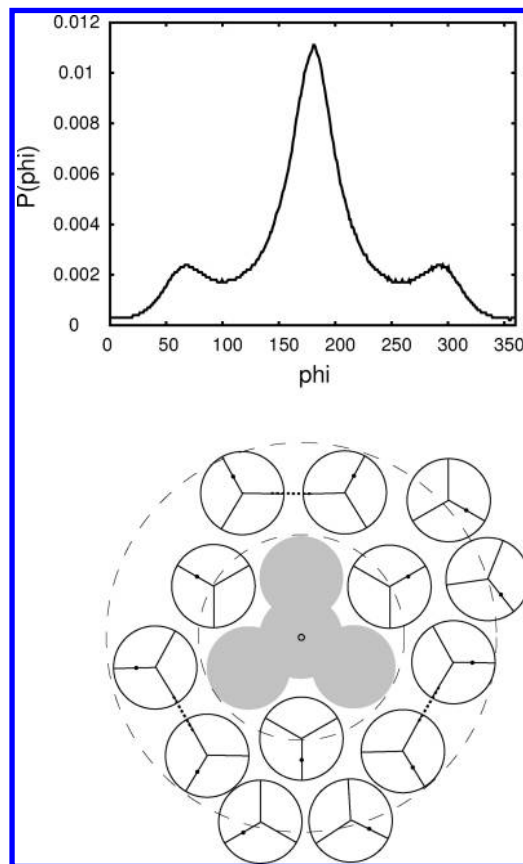


**Figure 5.** First two shells water–tetramethylammonium ion angle distribution function (upper panel) and a snapshot of the first two shells (indicated by thin broken lines) waters (lower panel) around the tetramethylammonium ion as obtained from MC simulation for the MB + dipole model.

hydrophobic cagelike structures around the methyl groups. To maximize water–water hydrogen bonding, the TMA model ion causes a structuring of the water orientations in the first two hydration shells, much like hydrophobic solutes do.<sup>24,41–44,46</sup> This is consistent with the experimental observations.<sup>43,44</sup>

Figure 5, upper panel, shows the angular distributions of first-shell water molecules around the TMA ion. The angle shown is calculated between the center of the TMA model ion and the water hydrogen bonding arm. This distribution arises from electrostatic water ordering. The water molecules are pointing the positive ends of their dipoles away from the positive charge on the TMA ion (corresponding to the angle  $180^\circ$  in Figure 5). Even though the TMA ion is large, and therefore would have

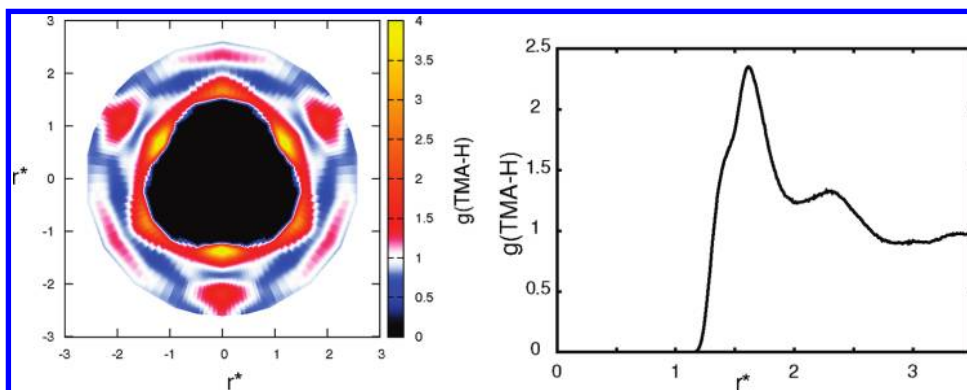


**Figure 6.** Monte Carlo simulation results for average (right panel) and orientation-dependent (left panel) hydrophobe–tetramethylammonium ion pair distribution function for hydrophobe of size  $\sigma_{\text{L}} = 1.5$ . Monte Carlo simulation results.

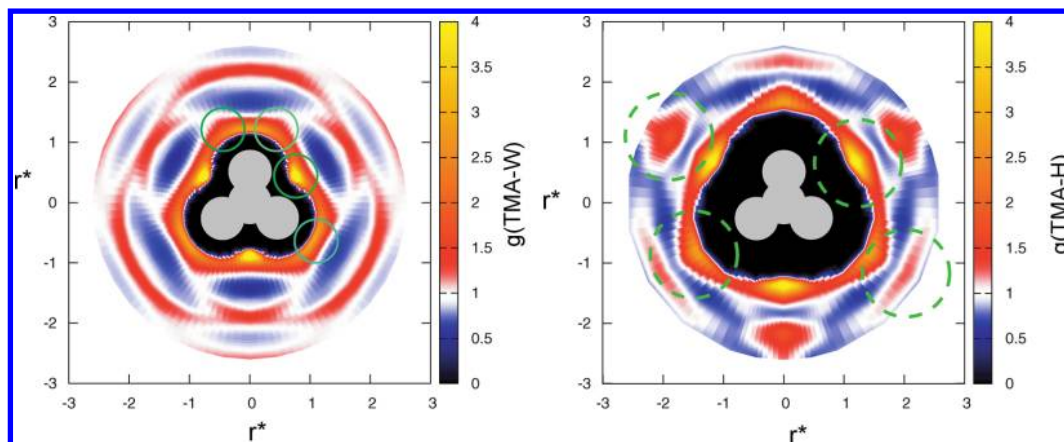


**Figure 7.** Orientation-dependent pair distribution function for water–tetramethylammonium ion (left panel) and hydrophobe–tetramethylammonium ion (right panel) for hydrophobe size  $\sigma_{\text{L}} = 1.5$ . Green circles denote the most probable location of water (left) and hydrophobe (right) molecules. Monte Carlo results.

low charge density on the outside, the first-shell water molecules are wedged and can approach much closer to the nitrogen, so from the perspective of the first-shell water molecules, the ion acts as if it had a high charge density.

For a clearer presentation, a snapshot of the TMA ion and its surrounding water molecules in the first two shells indicated by a thin broken line are shown in Figure 5, lower panel. First-shell waters have little or no hydrogen bonding because of the steric and electrostatic restrictions. If we calculate the liberation free energy,  $\Delta G_{\text{lib}}$ , of these first-shell waters around the TMA ion using a procedure described previously,<sup>24,47</sup> we get  $+0.51k_{\text{B}}T$ . This indicates that first-shell waters are strongly ordered (kosmotropic), similar to high-charge-density ions ( $\Delta G_{\text{lib}}$  for lithium ion, for example, is  $+0.48k_{\text{B}}T$ , while for sodium it is only  $+0.093k_{\text{B}}T$  and for cesium  $-0.42k_{\text{B}}T$ ).<sup>27</sup> This is consistent with the experimental values for Jones-Dole viscosity  $B$ -coefficients:  $+0.146$  for lithium,  $+0.085$  for sodium,  $-0.047$  for cesium, and  $+0.123$  for TMA ion.<sup>48</sup> Note that positive Jones-Dole  $B$  values are indicative for kosmotropes, while negative values are typical for chaotropic ions.<sup>27</sup> In the second shell around the TMA ion, however, there is a considerable cagelike structure, resulting from the influence of the first-shell waters and the hydrophobic effect arising from the methyl groups on the TMA ion.

To investigate the mechanism of salting-in, we looked at the potential of mean force between the model TMA ion and the hydrophobe (see Figures 6 and 7). The red areas in Figure 6 show an increased probability of finding the hydrophobe in the cavities after the second hydration shell. The TMA ion namely helps to orient the water molecules into cagelike structures,

forming cavities outside the second shell (Figure 5) where a large hydrophobe molecules can insert. In short, the strong electrostatic ordering of first-shell waters forces an arrangement of second-shell waters much like that of a “catcher’s mitt” or a “receptacle” of prestructured waters that can bind tightly to the hydrophobe. Nevertheless, the hydrophobe prefers to sit just outside the first hydration shell of water (blue areas in Figure 7, left panel), yet close to the TMA ion. The most favorable insertion sites for large hydrophobes are denoted as circles of thick green dashed lines in Figure 7, right panel. These observations are in agreement with previous findings:<sup>24,28</sup> salting-in occurs where the hydrophobic molecule loses some of its hydration water which is replaced by an ion. Between the first and second hydration shell, the microscopic water structure around the TMA ion enables a cavity to be readily formed (Figure 7).

Why are larger hydrophobes more salted-in by the TMA ion than smaller hydrophobes? Figure 8 shows the PMF for a larger hydrophobe than in Figure 6. Again, the hydrophobe prefers to sit just outside the first water shell of the TMA ion. Table 1 gives the computed free energies of insertion of the hydrophobes of different sizes into water, compared to the same quantities for TMA in pure water. Increasing the size of the hydrophobe reduces its  $\Delta\Delta G_{\text{ins}}$ . The TMA ion helps solvate the larger hydrophobes slightly more than smaller ones. A possible explanation is that due to its larger surface the probability of a larger hydrophobe to come into contact with the ion is higher. The TMA ion enables this contact by creating space in the solution. This can be seen if comparing the insertion volume of the TMA-model ion with its actual size. While the geo-

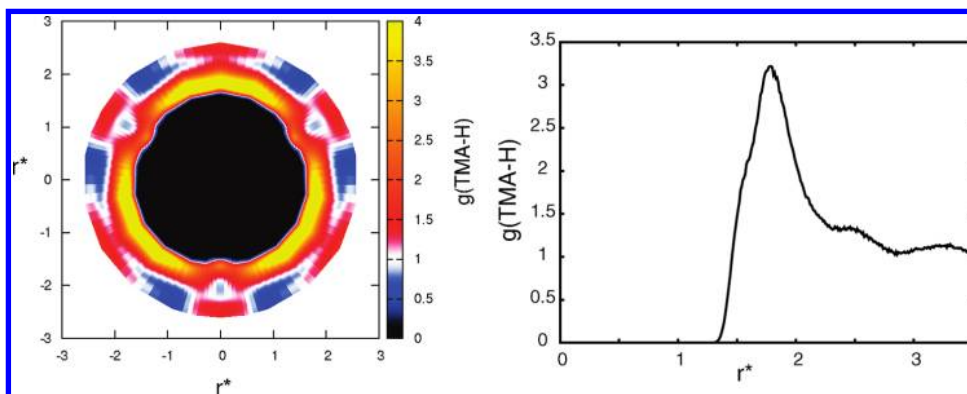


**Figure 8.** Same as in Figure 6 but for the hydrophobe size  $\sigma_{LJ} = 1.8$ .

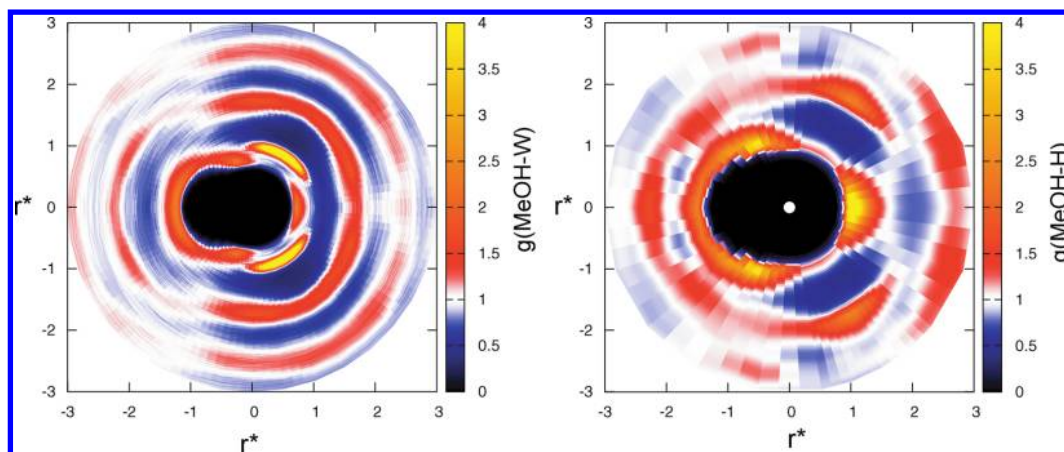


**Figure 9.** Orientation-dependent water–methanol ion (left panel) and hydrophobe–methanol (right panel) pair distribution function for hydrophobe size  $\sigma_{LJ} = 1.5$ . Monte Carlo results. The less intense color that appears on the left-hand sides of the panels, compared to the right-hand sides, is due to the asymmetry of the alcohol molecule.

metrically calculated “volume” of our TMA ion is 1.34, the insertion volume obtained from constant pressure Monte Carlo simulation for the same ion is 1.49, which is approximately 10% larger, creating that much more empty space in the solution. This is in qualitative agreement with the negative value of  $V_S - \bar{V}_S^0$  obtained experimentally for tetramethylammonium bromide solution in water.<sup>7</sup>

**3.1. Role of the Alcohol as a Cosolvent.** The salting-in has also been observed when certain alcohols<sup>17</sup> were added as cosolvents to aqueous solutions. The origin of this effect<sup>19</sup> is different from that for salts in pure water and as such not the primary scope of this work. While, as explained above, the change in the water structure brought about by the presence of the salt is an important factor in the salting-in process of electrolytes, an increase of the solubility of hydrophobic molecules in the presence of alcohols is interpreted in terms of the of alcohol–hydrophobe association.<sup>19</sup>

Here we were interested in whether the interaction between the hydrophobe and an alcohol molecule, which seem to be responsible for its increased solubility in mixed solvent,<sup>19</sup> could be captured by our model. For this reason, we performed computer simulations for the system containing a single molecule of model methanol in water, inserting into the system a single hydrophobe molecule of size  $\sigma = 1.5$ . The model for alcohol (methanol in this case) was described in our previous paper:<sup>49</sup> it consists of two Lennard-Jones disks of  $\sigma = 0.7$ , the first disk having two hydrogen bonding arms separated by an angle of  $120^\circ$  and the second disk’s center being on the rim of the first disk in the direction of the “missing” hydrogen bond. The parameters used in this calculation are as before (ref 49).

Methanol was chosen due to the availability of the experimental data for Setchenow  $k_S$  coefficients in the literature.<sup>16</sup>

The results are presented in Figure 9. The left side of this figure shows the relative water density around a methanol model molecule<sup>49</sup> and the right panel the angular-dependent potential of mean force between methanol and a hydrophobe of size  $\sigma = 1.5$ . As observed previously,<sup>49</sup> there is a high probability for a water molecule to form the hydrogen bond with the alcohol. The voids in the microscopic structure of water appear between the first and second shell of methanol hydration water. Figure 9 (right panel) on the other hand suggests that, although the probability of finding a hydrophobic molecule in these voids is increased, the most probable location for a hydrophobe is in contact with the hydrophobic part of the alcohol molecule. This conclusion is consistent with the mechanism used to explain the experimental results.<sup>9,18,19</sup>

#### 4. Conclusions

We explore here how tetramethylammonium ions help dissolve nonpolar solutes in water and why its Setschenow coefficient is negative. We perform NPT Monte Carlo simulations of the MB + dipole water model, which has previously been shown to capture both hydrophobic and ion solvation effects. We find that a first shell of water molecules wedges into the TMA ion. They are held tightly by the strong electrostatic interactions of the ion with water’s dipole. This first shell then causes structuring in a second shell to act as a receptacle for nonpolar solutes. In this way, the TMA ion facilitates the formation of cavities in its immediate vicinity

and can bind to hydrophobes more tightly than other waters can, helping in the solvation process. The model also captures the increased salting-in with increased solute size and/or increased temperature, as seen in experiments.

**Acknowledgment.** This study was supported by the Slovenian Research Agency fund (Programm 0103-0201) and by the NIH research Grant GM063592. B.H.-L. is thankful to A. Lajovic for the help in the preparation of the figures.

## References and Notes

- (1) Ben-Naim, A. *J. Phys. Chem.* **1965**, *69*, 3250–3253.
- (2) Wen-Hui, X.; Jing-Zhe, S.; Xi-Ming, X. *J. Thermochim. Acta* **1990**, *169*, 271–286.
- (3) McDevit, W. F.; Long, F. A. *J. Am. Chem. Soc.* **1952**, *74*, 1773–1777.
- (4) Hofmeister, F. *Arch. Exp. Pathol. Pharmacol.* **1888**, *24*, 247–260.
- (5) Kunz, W.; Henle, J.; Ninham, B. W. *Curr. Opin. Colloid Interface Sci.* **2004**, *9*, 19–37.
- (6) Baldwin, R. L. *Biophys. J.* **1996**, *71*, 2056–2063.
- (7) Long, F. A.; McDevit, W. F. *Chem. Rev.* **1952**, *51*, 119–169, and references therein.
- (8) Falabella, J. B.; Teja, A. S. *Ind. Eng. Chem. Res.* **2008**, *47*, 4505–4509.
- (9) Wen, W.-Y.; Hung, J. H. *J. Phys. Chem.* **1970**, *74*, 170–180.
- (10) Kunz, W. *Pure Appl. Chem.* **2006**, *78*, 1611–1617.
- (11) Kunz, W.; Lo Nostro, P.; Ninham, B. W. *Curr. Opin. Colloid Interface Sci.* **2004**, *9*, 1–18.
- (12) Cacace, M. G.; Landau, E. M.; Ramsden, J. J. *Q. Rev. Biophys.* **1997**, *30*, 241–277.
- (13) Thomas, A. S.; Elcock, A. H. *J. Am. Chem. Soc.* **2007**, *129*, 14887–14898.
- (14) Feillolay, A.; Lucas, M. *J. Phys. Chem.* **1972**, *76*, 3068–3072.
- (15) Ben-Naim, A. *J. Phys. Chem.* **1967**, *71*, 1137–1138.
- (16) Desnoyers, J. E.; Pelletier, G. E.; Jolicoeur, C. *Can. J. Chem.* **1965**, *43*, 3232–3237.
- (17) Ben-Naim, A. *J. Phys. Chem.* **1965**, *69*, 3245–3250.
- (18) Perez-Tejeda, P.; Delgado-Cobos, P.; Burgess, J. *Can. J. Chem.* **1990**, *68*, 243–246.
- (19) Nyssen, G. A.; Miller, E. T.; Glass, T. F.; Underwood, J.; Wilson, D. J. *Env. Mon. Assess.* **1987**, *9*, 1–11.
- (20) Tome, L. I. N.; Varanda, F. R.; Freire, M. G.; Marrucho, I. M.; Coutinho, J. A. P. *J. Phys. Chem. B* **2009**, *113*, 2815–2825.
- (21) Zangi, R.; Berne, B. J. *J. Phys. Chem. B* **2006**, *110*, 22736–22741.
- (22) Gurau, M. C.; Lim, S.-M.; Castellana, E. T.; Albertorio, F.; Kataoka, S.; Cremer, P. S. *J. Am. Chem. Soc.* **2004**, *126*, 10522–10523.
- (23) Smith, P. E. *J. Phys. Chem. B* **1999**, *103*, 525–534.
- (24) Kalra, A.; Tugcu, N.; Cramer, S.; Garde, S. *J. Phys. Chem. B* **2001**, *105*, 6380–6386.
- (25) Southall, N. T.; Dill, K. A. *J. Phys. Chem. B* **2000**, *104*, 1326–1331.
- (26) Southall, N. T.; Dill, K. A.; Haymet, A. D. J. *J. Phys. Chem. B* **2002**, *106*, 521–533, and references therein.
- (27) Hribar, B.; Southall, N. T.; Vlachy, V.; Dill, K. A. *J. Am. Chem. Soc.* **2002**, *124*, 12302–13311.
- (28) van der Vegt, N. F. A.; van Gunsteren, W. F. *J. Phys. Chem. B* **2004**, *108*, 1056–1064.
- (29) Pohorille, A.; Pratt, L. R. *J. Am. Chem. Soc.* **1990**, *112*, 5066–5074.
- (30) Deno, N. C.; Spink, C. H. *J. Phys. Chem.* **1963**, *67*, 1347–1349.
- (31) Hribar-Lee, B.; Vlachy, V.; Dill, K. A. *Acta Chim. Slov.* **2009**, *56*, 196–202.
- (32) Zhang, Y.; Cremer, P. S. *Curr. Opin. Chem. Biol.* **2006**, *10*, 658–663.
- (33) Thomas, A. S.; Elcock, A. H. *J. Am. Chem. Soc.* **2007**, *129*, 14887–14898.
- (34) Docherty, H.; Galindo, A.; Sanz, E.; Vega, C. *J. Phys. Chem. B* **2007**, *111*, 8993–9000.
- (35) Silverstein, K. A. T.; Haymet, A. D. J.; Dill, K. A. *J. Am. Chem. Soc.* **1998**, *120*, 3166–3175.
- (36) Dill, K. A.; Truskett, T. M.; Vlachy, V.; Hribar-Lee, B. *Annu. Rev. Biophys. Biomol. Struct.* **2005**, *34*, 173–199.
- (37) Bizjak, A.; Urbič, T.; Vlachy, V.; Dill, K. A. *Acta Chim. Slov.* **2007**, *54*, 532–537.
- (38) Widom, B. *J. Chem. Phys.* **1963**, *39*, 2808–2812.
- (39) Falabella, J. B.; Nair, A.; Teja, A. S. *J. Chem. Eng. Data* **2006**, *51*, 1940–1945.
- (40) Pegram, L. M.; Thomas Record, M., Jr. *J. Phys. Chem. B* **2008**, *112*, 9428–9436.
- (41) Krienke, H.; Vlachy, V.; Ahn-Ercan, G.; Bako, I. *J. Phys. Chem. B* **2009**, *113*, 4360–4371.
- (42) Slusher, J. T.; Cummings, P. T. *J. Phys. Chem. B* **1997**, *101*, 3818–3826.
- (43) Garcia-Tarres, L.; Guardia, E. *J. Phys. Chem. B* **1998**, *102*, 7448–7454.
- (44) Turner, J. Z.; Soper, A. K.; Finney, J. L. *J. Chem. Phys.* **1995**, *102*, 5438–5443.
- (45) Marcus, Y. *J. Solution Chem.* **2008**, *37*, 1071–1098.
- (46) Garde, S.; Hummer, G.; Paulaitis, M. E. *J. Chem. Phys.* **1998**, *108*, 1552–1561.
- (47) Chong, S. H.; Hirata, F. *J. Phys. Chem. B* **1997**, *101*, 3209–3220.
- (48) Marcus, Y. *Ion Solvation*; John Wiley: New York, 1985.
- (49) Hribar-Lee, B.; Dill, K. A. *J. Acta Chim. Slov.* **2006**, *53*, 257–263.